256
10/4/79

Hd. 114

UCRL-52784

CONTAINMENT CALCULATION FOR BURZET

R. W. Terhune
L. R. Moreno

May 29, 1979

MASTER

Work performed under the auspices of the U.S. Department of Energy by the UCLLL under contract number W-7405-ENG-48.

LAWRENCE
LIVERMORE
LABORATORY
University of California/Livermore

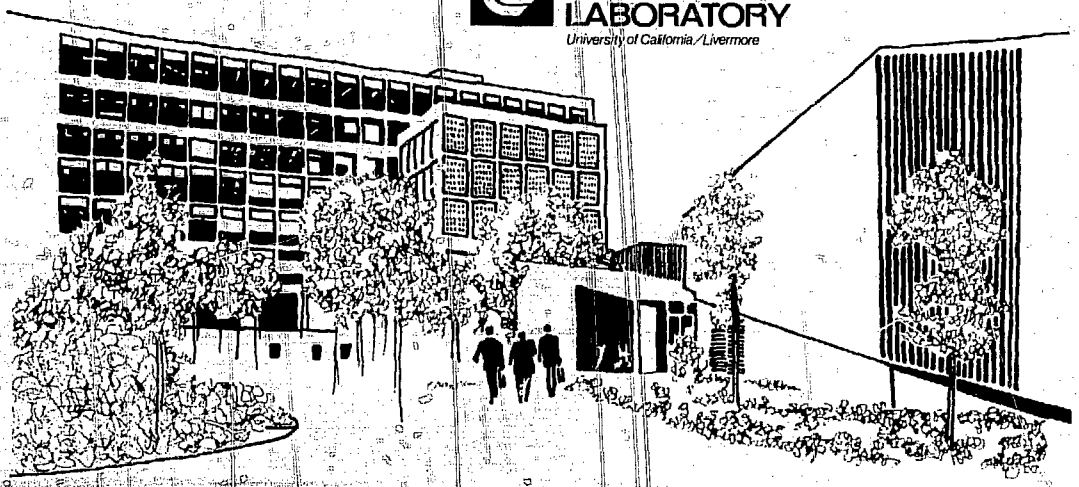

Distribution Category
UC-11

LAWRENCE LIVERMORE LABORATORY
University of California / Livermore, California / 94550

UCRL-52784

CONTAINMENT CALCULATION FOR BURZET

R. W. Terhune
L. R. Moreno

MS. date: May 29, 1979

CONTENTS

LIST OF ILLUSTRATIONS

LIST OF TABLES

CONTAINMENT CALCULATION FOR BURZET

R. W. Terhune
L. R. Moreno

University of California, Lawrence Livermore Laboratory
Livermore, California 94550

ABSTRACT

Burzet is a proposed intermediate-yield underground test of a nuclear explosive at the Nevada Test Site. The possible existence of a high Paleozoic scarp and fault within 100 m of the proposed working point created concern as to their effect on the containment of the radioactive gases. A calculation of the expected stress wave interaction at the scarp and fault demonstrates that the effects are negligible. Results of the calculation are those expected from an event in a homogeneous media and are thus consistent with good containment experience on numerous previous detonations of similar yield, depth of burial, and medium properties.

INTRODUCTION

A Paleozoic scarp and fault west of the Burzet working point creates a large impedance contrast and a possible zone of material weakness. The fault and scarp were thought to be sufficiently close to the Burzet working point that a calculational examination of their effects on the development and stability of the "containment cage" was deemed prudent. The calculation presented here is based on an early version (November, 1978) of the cross section for the test hole (Ue4ac), which has since been revised, as shown in Fig. 1.[1] Figure 1, therefore, shows the position of the scarp and fault relative to the working point, both for the calculation and as they are currently shown on the cross section.

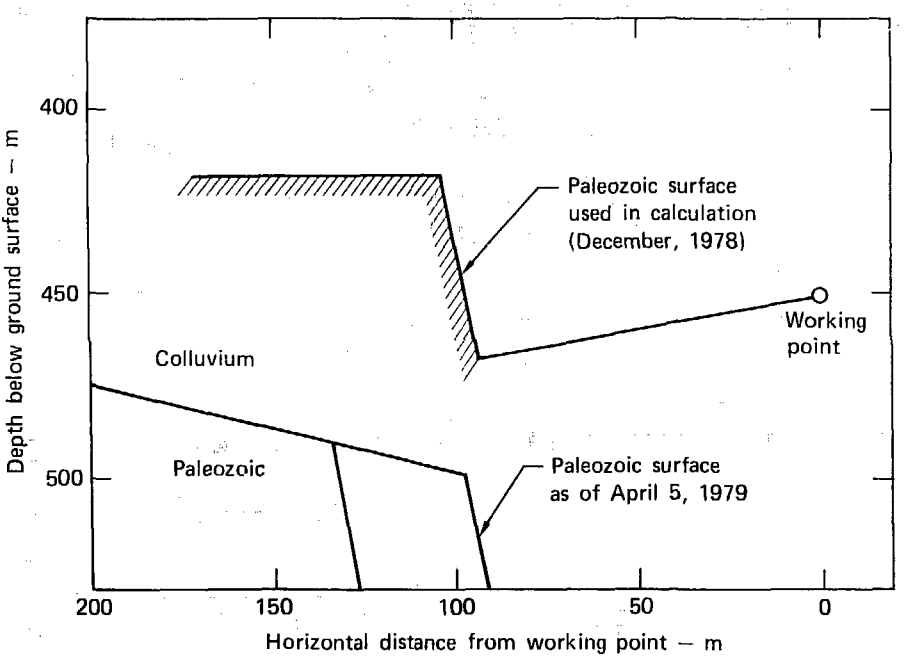

FIG. 1. Cross section showing fault and scarp as assumed for the calculation and as currently placed.

The concerns which the calculation was designed to address were:

- Enhancement of ground motion above the cavity due to a near-horizontal reflected stress wave from the Paleozoic surface. A sufficiently strong reflected stress wave could possibly produce nonsymmetrical ground motion above the cavity, which may affect the stability of the containment cage. In addition, enhanced ground motion could possibly delay the onset of the containment cage to a point where it would be affected by the reflected surface tensile wave.
- Divergent flow of material along the surface of the Paleozoic scarp, producing a region of open voids between the scarp and the cavity and a possible escape path for the cavity gas to the fault.
- Shear displacement along the fault and possible extension of the fault into the spall zone.

We will first present the calculational model used in the analysis, followed by the calculational results for each of the three major concerns. None of the concerns developed in the calculation. The Paleozoic scarp and fault as modeled had a negligible impact on the development and stability of the containment cage.

As shown in Fig. 1, the current configuration of the scarp and fault differs from the one modeled. However, we argue that the current configuration does not introduce any additional containment concerns and that the model adequately addresses all containment concerns of the current configuration.

COMPUTATIONAL MODEL

The calculation was done with the TENSOR[2,3] code. The TENSOR code is a two-dimensional scheme that integrates the conservation equations of continuum mechanics to solve problems involving stress-wave propagation. The rock constitutive models in the code take into account pore collapse, both ductile and brittle (strain-softening) failure, tensile failure with crack opening and closure, and rock melt and vaporization.

To simulate the characteristic of a stress wave arising from a detonation of a nuclear explosive, the energy source must be modeled as a sphere. This requires that the geometry of the calculational grid be axially symmetric in cylindrical coordinates, with the axis of symmetry passing through the center of the energy source.

For most calculations of this type the axis of symmetry is oriented to coincide with the emplacement hole axis. This, however, would rotate the Paleozoic scarp in such a manner that the model would better represent an explosive in a cannon barrel than the actual situation.

A more representative model is achieved by orienting the axis of symmetry normal to the fault plane and modeling that portion of the geologic structure between the axis of symmetry and the free surface. Thus, all horizontal features of the geologic structure are transformed into the curved cylindrical surfaces of the frustums of a right cone. The planar face of the scarp along the fault is modeled by the top of the frustum of a cone and has a radius of 50 m. The planar fault is represented by a 10-m-thick disk with a radius of 160 m. Figure 2 shows the region of interest, as modeled for the calculation, and the materials of each region. The minimum distance from the working point to the fault is 85 m; the minimum distance to the Paleozoic scarp is 95 m. The entire grid of the calculation models the geology 3000 m to the west of the working point and 1200 m to the east. The overburden stress was modeled as a hydrostatic stress proportional to the vertical depth below the free surface.

The advantage of this model is that the primary reflective surfaces of the Paleozoic scarp and fault remain planar, resulting in a reasonably realistic modeling of the phenomenology related to the primary containment concerns. One major disadvantage is that any flow of material around the scarp corner is enhanced because of its finite size in all directions. Another important disadvantage is that the reflective tensile wave from the free surface converges on the axis of symmetry, resulting in a deeper spall depth and stronger tensile wave on the containment cage than would be expected from a plane horizontal surface.

Three material equations of state (EOSs) were used in the problem to describe the Paleozoic rock, the fault, and the alluvium. The high-impedance Paleozoic rock EOS was inferred from measurements on numerous samples of similar rock from other parts of the test site.[1] The fault material was assumed to be saturated clay-enriched tuff with properties identical to those used in the Baneberry calculations.[4] The third medium was alluvium, whose EOS was based on preliminary measurements of the geophysical properties.[1] The average strength properties were determined from cavity radii measurements.[5] After the calculations were half completed, strength measurements on samples

from Ue4ah[6] were made. They showed excellent agreement with those assumed in the calculation for alluvium, as depicted in Fig. 3. Table 1 gives the EOS parameters for each medium used in the calculation. The final measured bulk density is slightly lower than the preliminary measurements.[7] This resulted in the calculated air-filled porosity being 10 to 15%, instead of the 4% used in our model. The lower air-filled porosity used in the model resulted in a stronger, less attenuated stress wave and larger ground motion than would a calculation using the higher air-filled porosity.

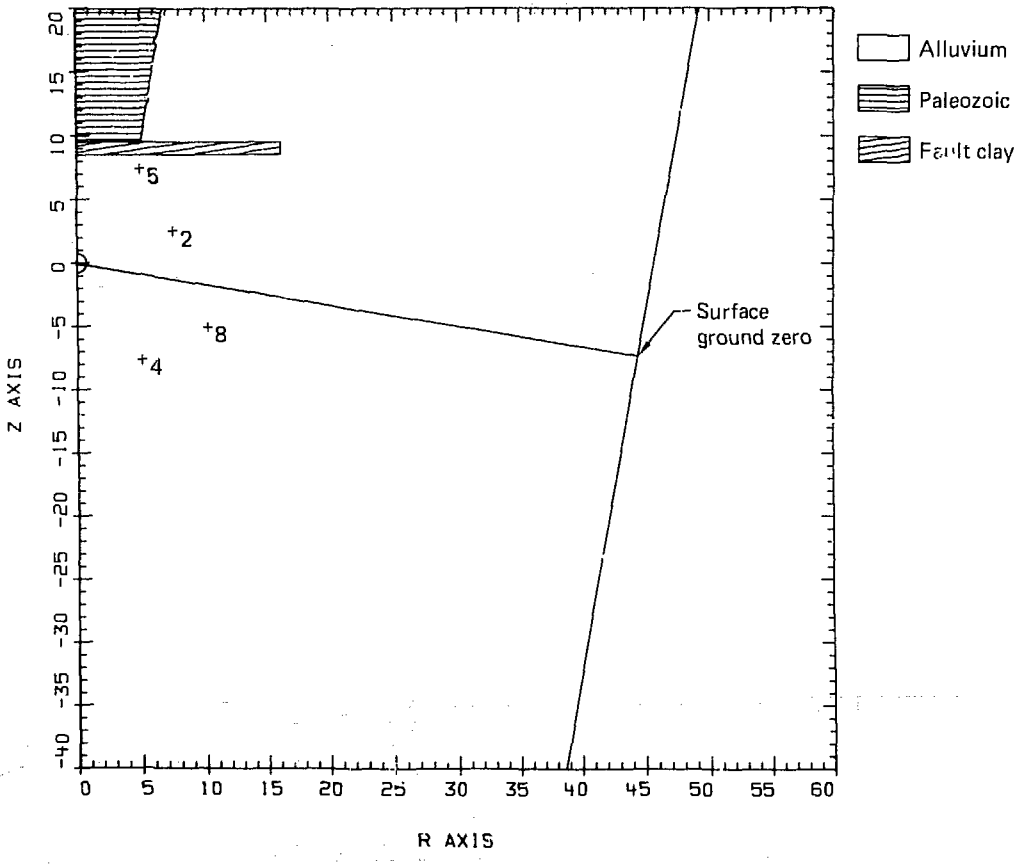

FIG. 2. Region of the fault and scarp, as modeled for the calculation, showing the three material regions. Time histories were obtained for the numbered locations. The units for both axes are tens of meters.

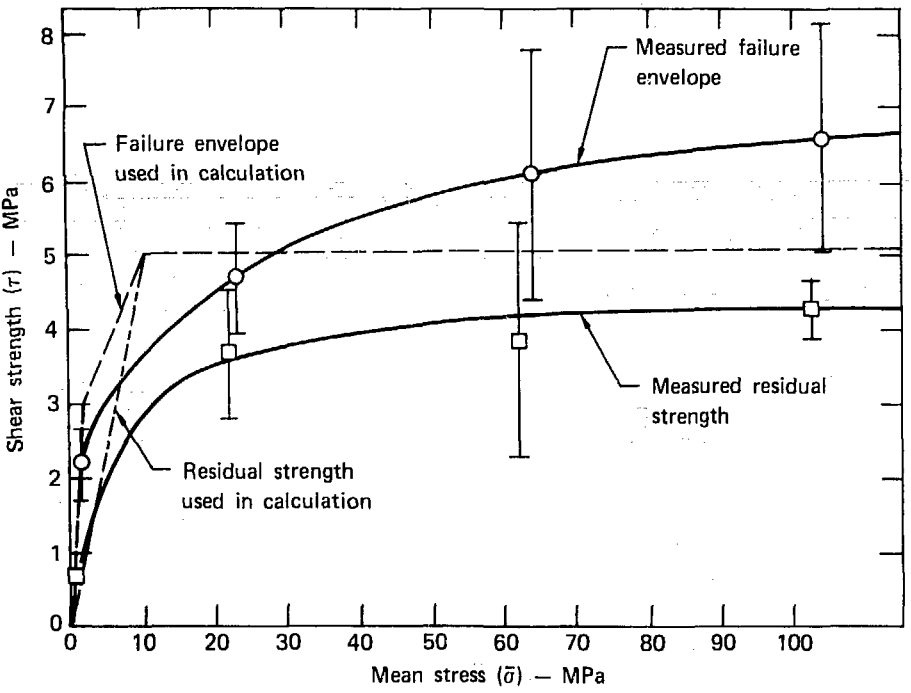

FIG. 3. Variation of shear strength (τ) with mean stress ($\bar{\sigma}$). Each data point is the mean of eight tests of initial failure (circles) and of residual strength (squares). The error bars represent one standard deviation. Test samples were drawn from depths between 1634.5 and 1642.5 m. The broken lines show the failure envelope and the residual strength assumed in the calculation. Above 10 MPa, the two lines coincide.

TABLE 1. Physical properties for modeled materials.

Property	Alluvium	Paleozoic	Fault clay
In situ density, Mg/m^3	2.01	2.65	2.0
Grain density, Mg/m^3	2.54	2.81	2.78
Weight % water	13.9	3.2	21.9
Air-filled porosity, %	4.0	0	0
Compressional velocity, m/s	1643	5000	1898
Elastic limit, bars	80	1000	10
Shear strength, bars	50	750	20
Poisson's ratio	0.3	0.2	0.42

The energy input was the maximum credible yield for Burzet, incorporated into the Bubble model[8] for the source. The calculational grid was moderately fine zoned, using 70 radial L lines and 156 K lines. The zone size increased geometrically from the source outward, with 0.45-m zones near the source and 9.0-m zones at surface ground zero.

CALCULATIONAL RESULTS

We will report the results of the calculations as they pertain to the primary areas of concern in the order listed. Each containment concern will then be discussed in terms of the current configuration of the scarp.

In general, the calculation produced a well-defined stress wave characteristic of those measured from numerous nuclear explosions. The initial rise of the stress wave to the peak was defined calculationally with 30 or more zones within the region of interest at all times. The duration of the calculation relevant to the primary purpose of the study (to assess the effect of the scarp on the containment features) was less than 0.5 s. At 0.520 s, the convergent tensile wave from the free surface converged on the axis of symmetry. After 0.52 s, the calculation became less relevant to the Burzet event. At the Burzet depth of burial, the tensile reflection from a plane free surface was not considered a threat to a well-developed and stable containment cage. The calculation was continued to a total time of 1 s. Although the convergent tensile wave did severely degrade the containment cage temporarily, it had recovered fully by 0.7 s.

STRESS WAVE REFLECTIONS FROM PALEOZOIC SCARP

The time interval during which the reflection from the Paleozoic scarp would affect the earth motion around the cavity was the first 0.2 s. Figure 2 shows the location of three grid points (5, 2, 8) at which time histories of velocity, displacement, and stress were monitored. Figure 4 shows the pressure histories at the three grid points. The reflected stress wave is clearly evident, but it is a very small perturbation on the back side of the outgoing stress wave. This was expected; however, the reflected stress wave is almost normal to the outgoing wave. We were concerned that this situation might cause some asymmetrical earth motion.

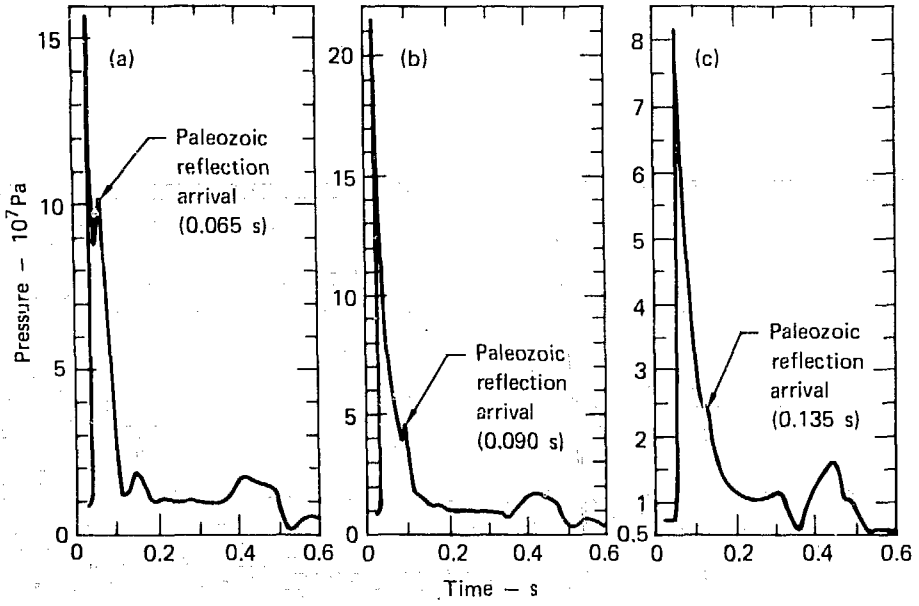

FIG. 4. Pressure time histories at grid locations shown in Fig. 2: (a) 5, (b) 2, and (c) 8.

Figure 5 shows the direction of earth motion at a time when the effects from the reflection was expected to be most noticeable along the z-axis. The solid angular curve above the expanding cavity shows the region through which the reflected wave has passed. All velocity vectors are radial to the source center except those near the Paleozoic boundary. The velocity vectors remained radial well past any period during which the Paleozoic reflection could have any effect. Thus, we conclude that the reflections from the Paleozoic boundary would not adversely affect the earth motion or the formation of the containment cage.

Some tensile fracturing occurred near the cavity on the axis of symmetry, due to the reflected wave impinging on the cavity surface. However, the fractures closed so rapidly that edits at 20-ms intervals did not reveal any open fractures. The current position of the Paleozoic scarp is well below the work point so that stress waves impinging on the side of the scarp will be reflected downward below the work point, and those impinging on the top of the scarp will be reflected away from the work point and the containment cage

region. Thus, the effects of the reflections on the containment of Burzet are likely to be much less than those modeled and are not expected to produce a containment hazard.

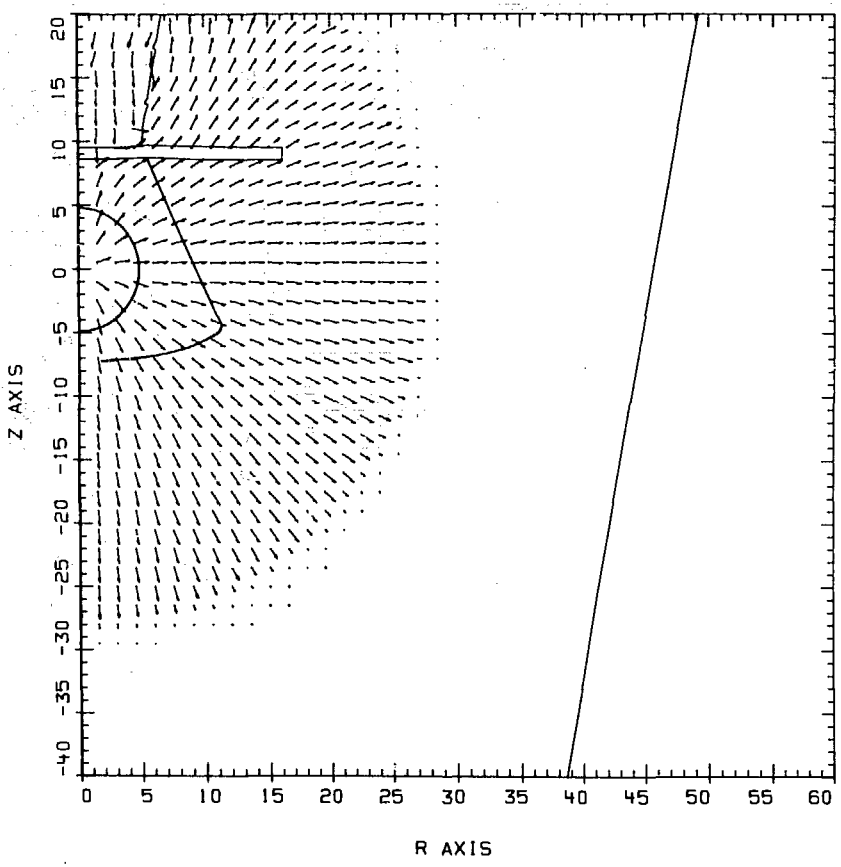

FIG. 5. Velocity vectors showing direction of earth motion at 0.14 s. Units for both axes are tens of meters.

DIVERGENT FLOW ALONG THE SCARP BOUNDARIES

There are two regions where divergent flow could possibly develop, thus reducing the stress state or opening fractures between the cavity and the fault. One is at the intersection of the axis of symmetry with the Paleozoic surface; the other is at the corner of the Paleozoic scarp where the top of the scarp intersects the fault.

Figure 5 shows that material flow does occur along the scarp-fault interface and around the corner of the scarp. This general flow pattern continued to 0.28 s with diminishing magnitude and slowly evolved into the flow pattern shown in Fig. 6 at 0.30 s. The flow pattern of Fig. 6 was of short duration, as all velocity vectors within 200 m of the working point reversed at 0.34 s, initiating the development of the containment cage. Our main concern was that the flow tangent to the scarp-fault interface might produce sufficient stress relief to be a containment hazard in this region. Figure 7 is an isobar map of the stress field at 0.2 s. The isobars are reasonably symmetrical around the cavity. The slight deviation in the 10-MPa

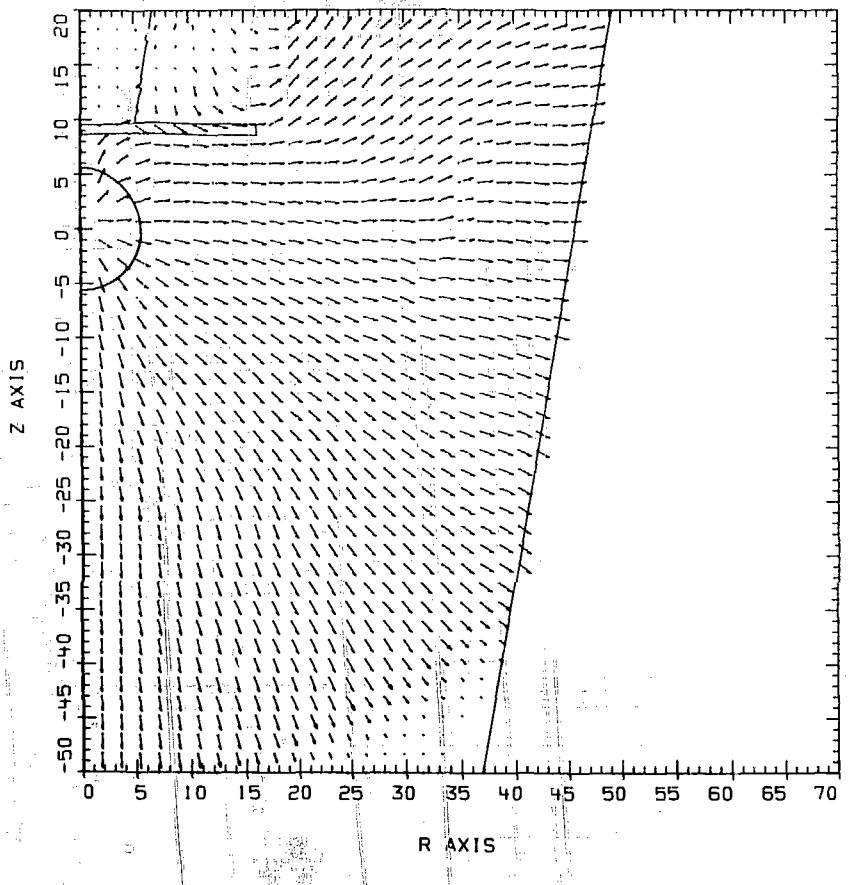

FIG. 6. Velocity vectors showing direction of earth motion at 0.3 s. Units for both axes are tens of meters.

isobar line near the corner of the scarp suggests that some stress relief occurs because of the material flow. However, the stress relief is very small, and the total stress in this region remains approximately twice the cavity pressure until the onset of the containment cage. Figure 4(a) shows that the pressure is essentially constant during the interval from 0.18 to 0.34 s. Thus, we conclude that the flow along the scarp boundaries would not produce a containment hazard.

The scarp as modeled is expected to have a larger perturbation on the stress field than the actual scarp. The surfaces of the actual scarp are farther from the work point than those modeled, and the change in the

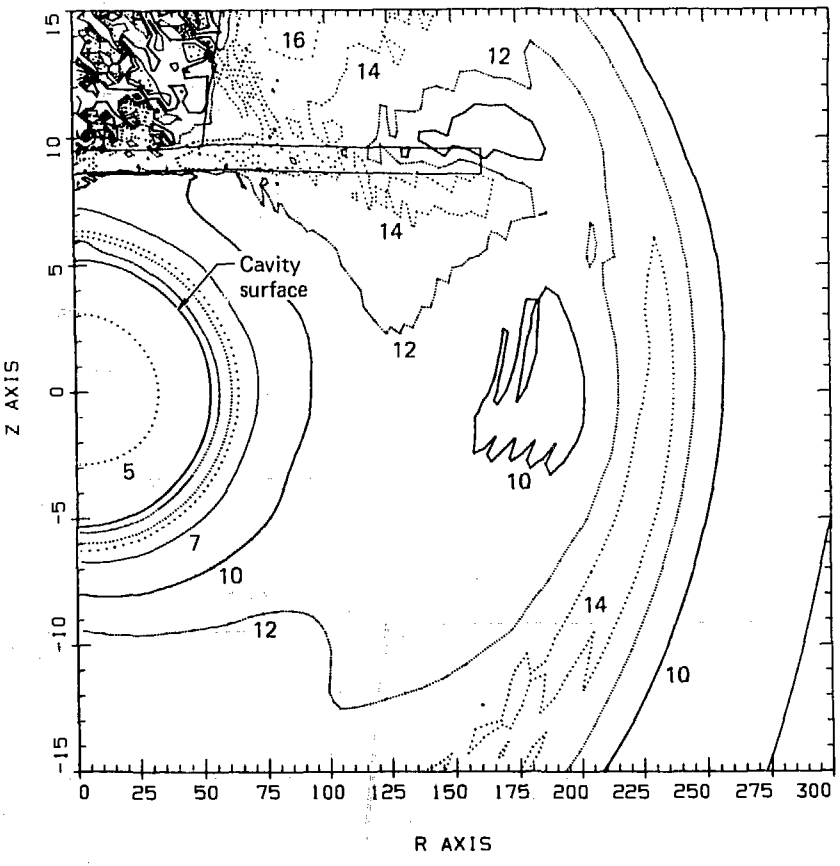

FIG. 7. Isobar map of stress field at 0.2 s. Numbers on the isobars denote the pressure in MPa. Units for the z-axis are tens of meters; for the r-axis, meters.

direction of flow will be much less severe. In addition, the flow in the model is around the corner of a cylinder, whereas the edge of the actual scarp is like the corner of an infinitely long wedge. Consequently, we do not expect any adverse effects on containment due to divergent flow around the scarp.

SHEAR DISPLACEMENT AND FAULT EXTENSION

The fault was modeled as a 10-m-thick disk extending 100 m into the alluvium above the top surface of the Paleozoic scarp. In comparison to the surrounding alluvium, the fault material was modeled as a very weak saturated clay. Our intent was to simulate a weak shear zone capable of sustaining large shear displacements across it. Our primary concern was that the shear action along the fault might produce conditions that could be interpreted as open fractures along the fault and/or an extension of the fault plane into the alluvium toward the free surface and spall zone.

The interpretation of the calculational results for fault extension is based on a comparison of the displacement vectors with the displacement contours in the region between the fault tip and the free surface. An example of this method of interpretation is the calculation for Baneberry,[4] where the fault is known to have extended to the surface. Figure 8 is the material grid of the Baneberry calculation with the displacement vectors and magnitude contours superposed. The displacement contours provide a measure of the gradient of the displacement field. The displacement magnitude contour lines in Fig. 8 are at intervals of 0.2 m from 0.2 m to 2.0 m. The contour lines are closely spaced within the fault and above it, indicating a high displacement gradient. Both the contour lines and the displacement vectors are parallel to a line extending along the fault to the surface. The high gradient and the orientation of both the vectors and contour lines suggest that a strong shearing action occurred within the fault and above it. This is interpreted as a condition that could result in an extension of the fault.

Figures 9 and 10 show similar plots for the Burzet calculation at times of 0.3 s and 0.48 s, respectively. Figure 9 is at a time when the displacements on the far side of the fault are at a maximum, and Fig. 10 is at a time following rebound, when the surface tensile wave front is near the cavity boundary. The shear displacement across the fault is approximately 1 m, but the displacement vectors are normal to the contour lines and essentially

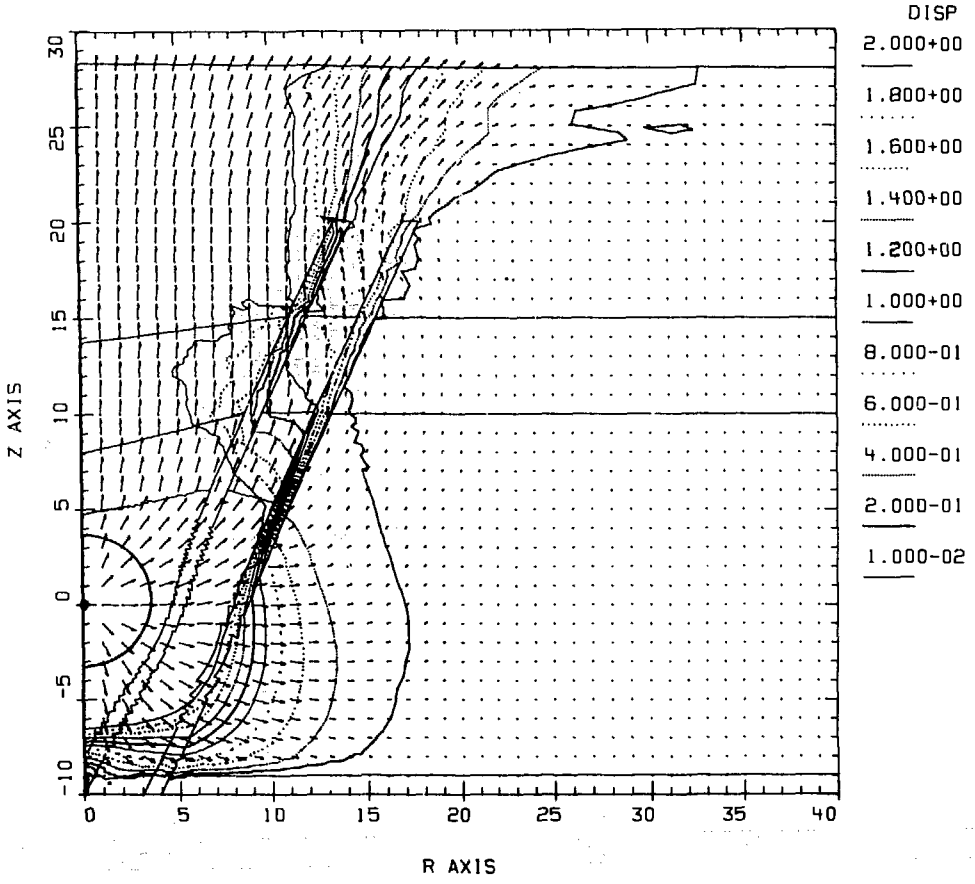

FIG. 8. Displacement vectors and contours from the Baneberry calculation (Ref. 4) at 0.9 s. Units for both axes are tens of meters. Units for the displacement contours in the key are meters.

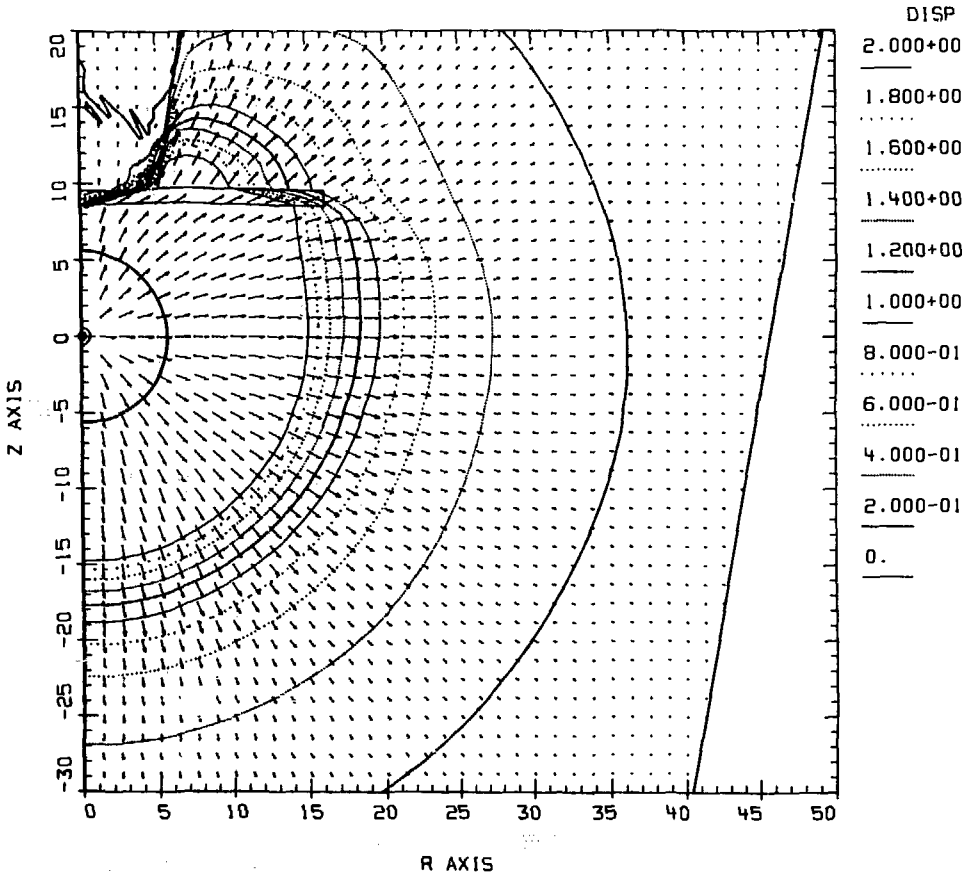

FIG. 9. Displacement vectors and contours at 0.3 s. Units for both axes are tens of meters. Units for the displacement contours in the key are meters.

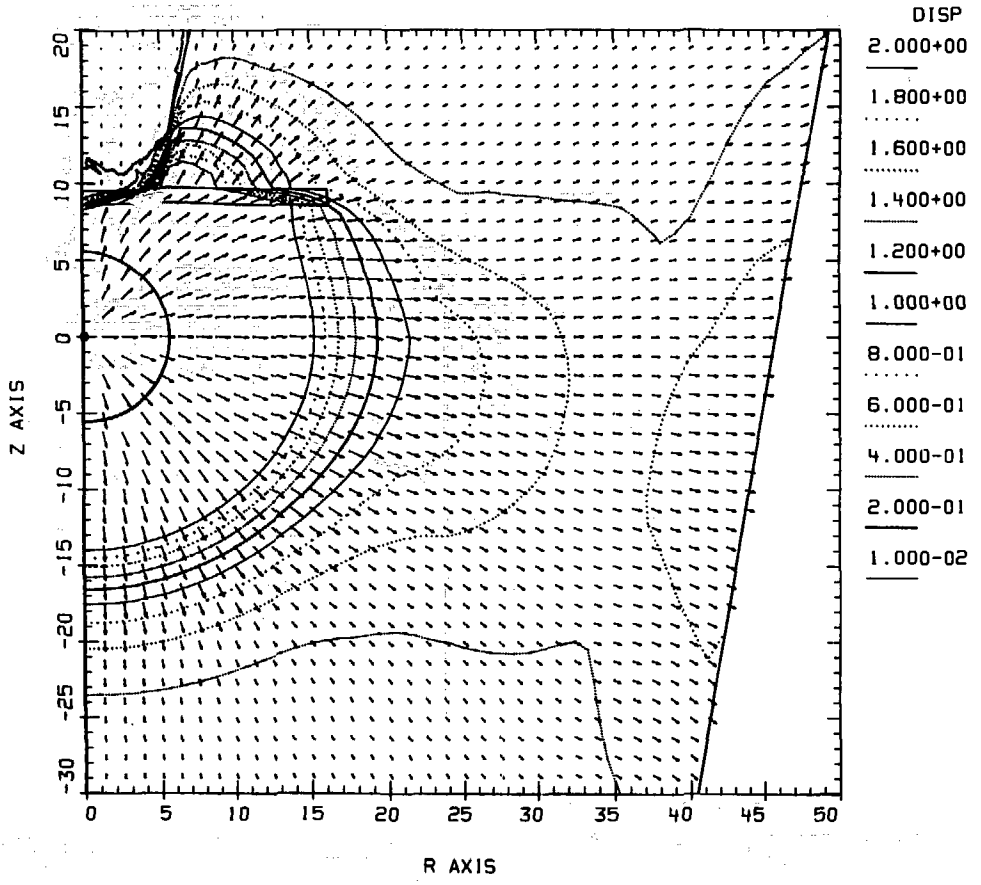

FIG. 10. Displacement vectors and contours at 0.48 s. Units for both axes are tens of meters. Units for the displacement contours in the key are meters.

radial from the working point in the regions outside the fault. This condition is interpreted as being a compression or expansion of the grid zones, with very little shear action occurring in the regions outside the fault. These conditions suggest that the fault will not extend or propagate toward the surface or spall zone.

The conditions within the fault were also closely monitored during the calculation for any tendency of open or tensile fractures to occur. None were found, as the stress state within the fault exceeded 10 MPa until 0.52 s, when the convergent surface tensile wave caused the failure of the region on the axis of symmetry. Figure 11 is a cumulative plot of all regions that failed

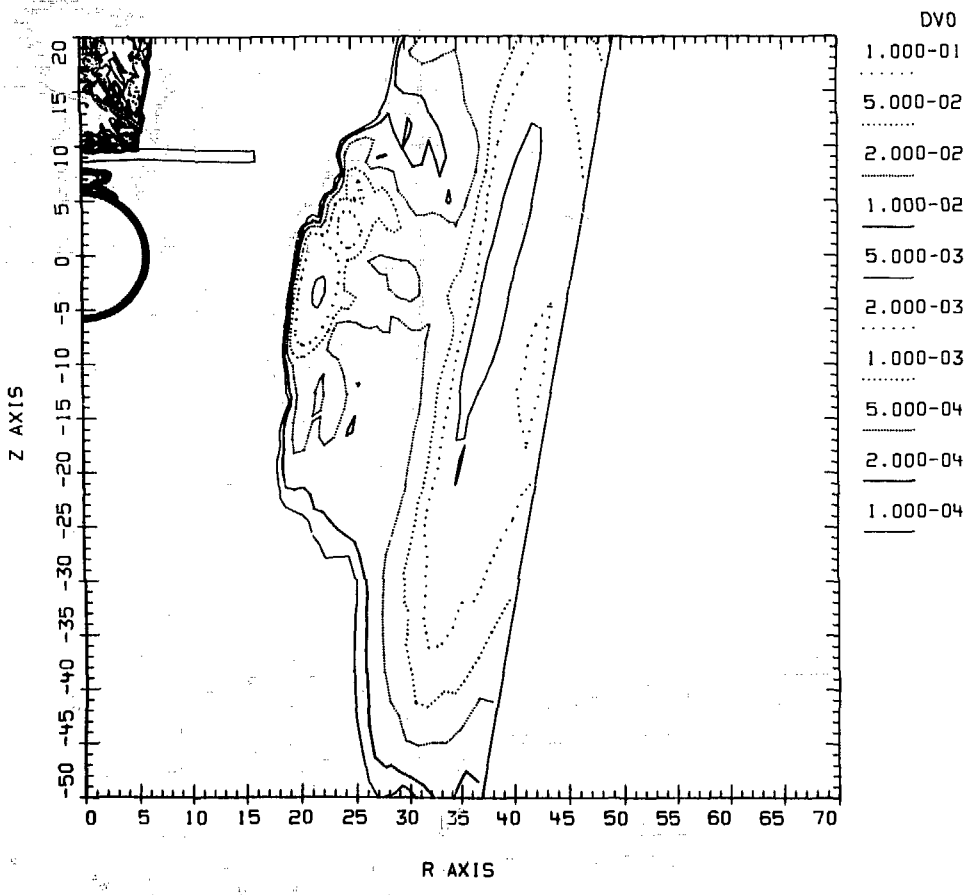

FIG. 11. Regions of tensile fracture occurring in the interval between 0.0 and 0.48 s. Units for both axes are tens of meters. The strain contours in the key are dimensionless.

in tension during the elapsed time from 0.0 to 0.48 s. Tensile failure occurred near the cavity due to the Paleozoic reflected wave impinging on the cavity surface, and also in the Paleozoic region shown in the figure. The limits of tensile failure due to spall at the surface are also shown. The spall depth of 250 m is larger than expected, because of the convergent tensile wave from the surface. Note that the fault is free from any tensile fractures, as is the region between the cavity and spall zone. The region between the cavity and spall zone remains free of tensile fractures during the entire calculation to 1 s.

CONTAINMENT CAGE DEVELOPMENT

The timing of the containment cage development is evident from the hoop stress histories at grid locations outside the cavity, as shown in Fig. 12. The onset of the containment cage occurred at 0.34 s and peaked at 0.41 s, with a maximum stress of 20 MPa, which is approximately four times the calculated cavity pressure. Figure 13 shows an isoplot of the residual hoop stress around the cavity at 0.48 s. At this time, the stress state satisfied all the criteria for a strong stable containment cage. The effects of the arrival of the convergent surface tensile wave on the residual stress is shown in Fig. 12.

The magnitude of the tensile wave and its effect on the residual stress is an artifact of the model's geometry. The arrival of the convergent surface tensile wave was the primary constraint on the time duration over which the calculational model was valid. However, we chose to continue the calculation to determine if the residual stress would recover from such a severe (and unrealistic) rarefaction from the surface. The residual stress did recover, increasing with time, and reformed a strong, stable, symmetric containment cage. Figure 14 shows an isoplot of the residual hoop stress at 0.74 s. This recovery of the residual stress state is indicative of the strength and stability of the containment cage.

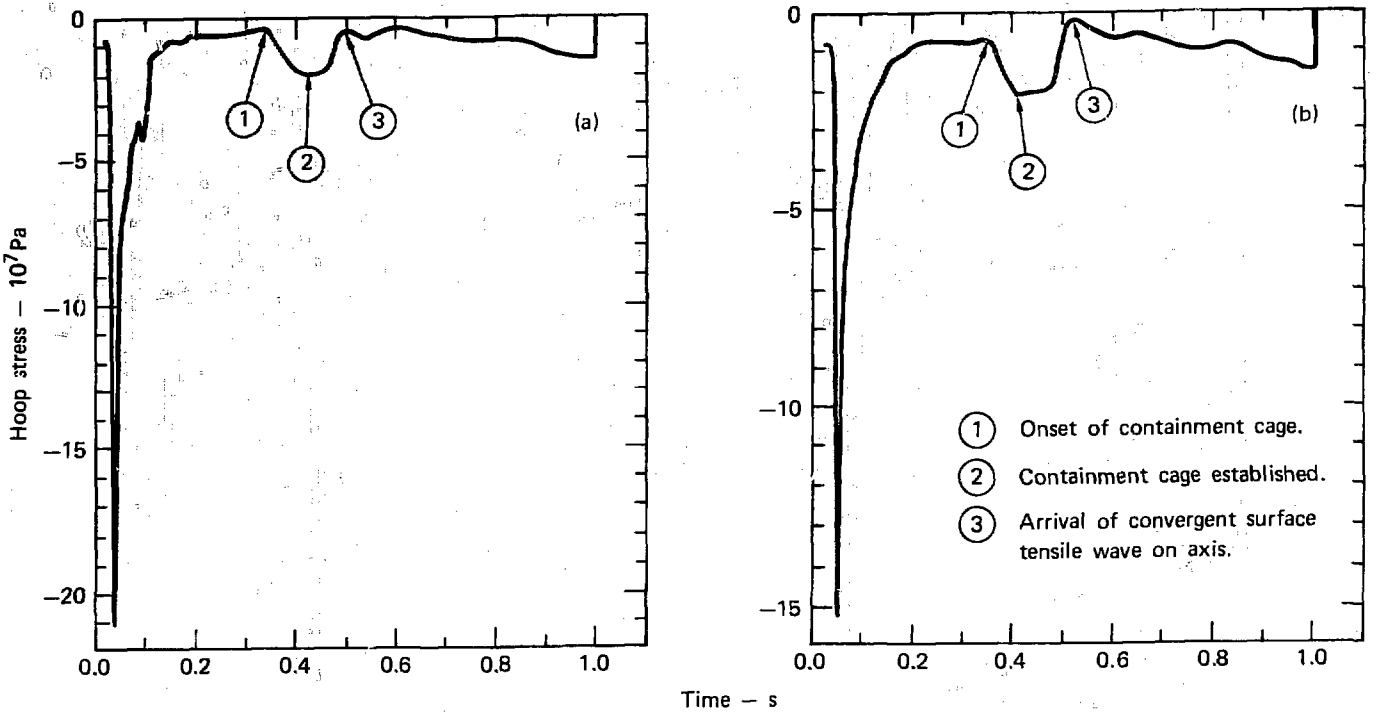

FIG. 12. Hoop stress time histories at grid locations shown in Fig. 2: (a) 2, and (b) 4.

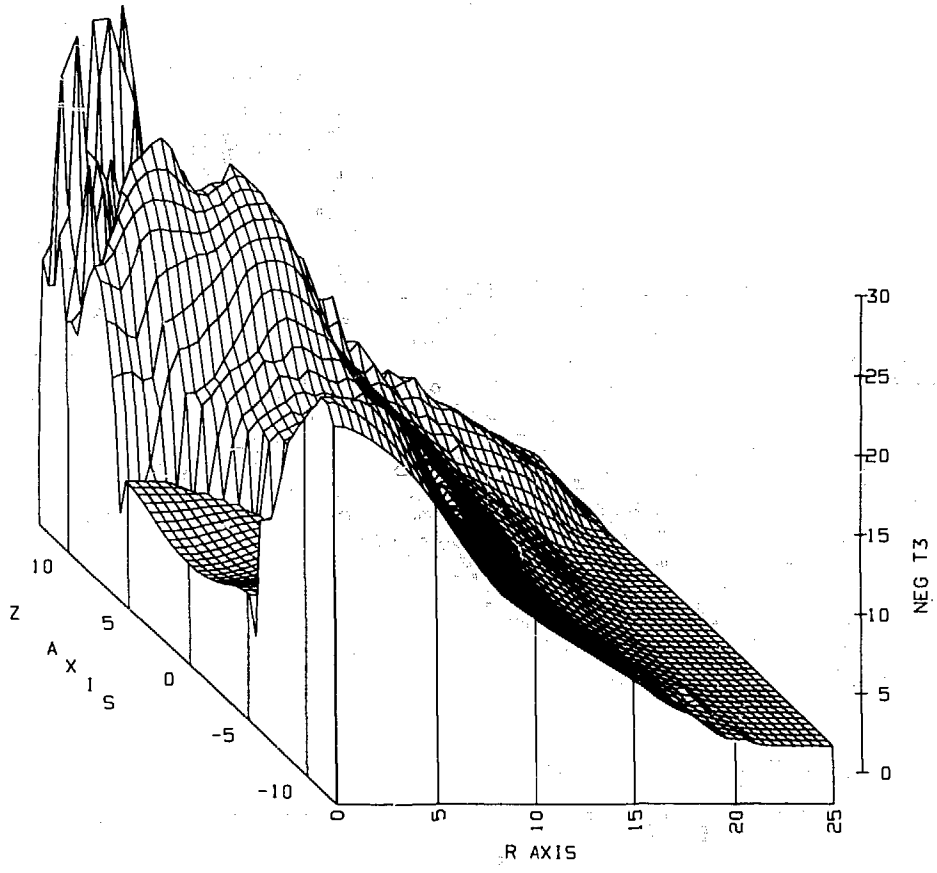

FIG. 13. Isoplot of the residual hoop stress around the cavity at 0.48 s. Units for the x- and r-axes are tens of meters; for the vertical axis, 10^6 Pa.

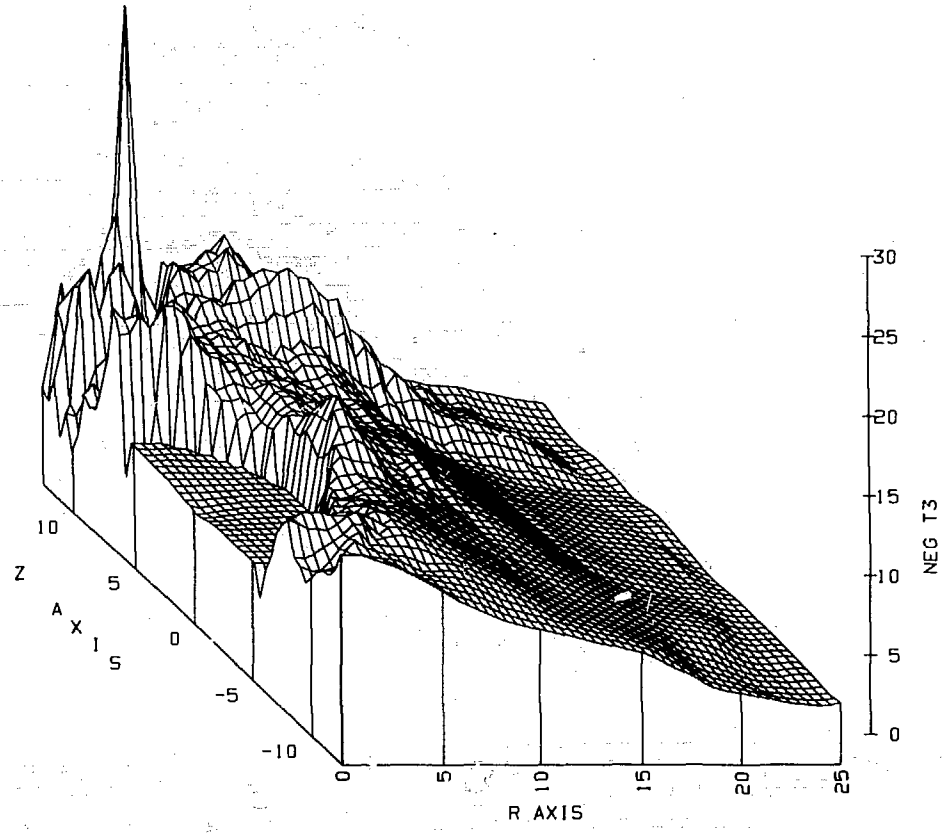

FIG. 14. Isoplot of the residual hoop stress around the cavity at 0.74 s. Units for the x- and r-axes are tens of meters; for the vertical axis, 10^6 Pa.

CONCLUSIONS

We believe that the calculational model adequately accounts for the phenomenology due to the Paleozoic scarp and fault near the Burzet working point, which enables us to evaluate their impact on the containment of Burzet. An assumption inherent in the analysis is that (excluding the scarp and fault) we would expect Burzet to be contained--an assumption based on relevant previous experience in this yield range and depth of burial. The purpose of the calculation was to determine if the scarp or fault would produce any anomalies in the stress, strain displacement, or velocity fields, or would alter the timing of any phenomena familiar from our calculational experience of previous well-contained events.

The analysis of the calculation concentrated on three possible effects of the scarp and fault to evaluate their interaction with the containment cage. The results of the calculations indicate that no serious degradation of the containment cage occurs for the duration of the calculations. The reflections from the Paleozoic scarp do not result in asymmetrical earth motion or affect the timing of the onset of the residual hoop stress that forms the containment cage. The flow around the scarp surfaces do not degrade the stress state around the cavity. The fault shows no tendency to open or to extend toward the surface. In summary, the calculational results satisfy all the criteria for containment and show no adverse effects due to the scarp or fault.

REFERENCES

1. H. L. McKague, private communication (1979).
2. D. E. Burton and J. F. Schatz, *Rock Modeling in TENSOR74*, Lawrence Livermore Laboratory, Livermore, Calif., UCID-16719 (1974).
3. G. Maenchen and S. Sack, *The TENSOR Code*, Lawrence Livermore Laboratory, Livermore, Calif., UCRL-7316 (1963).
4. R. W. Terhune, H. D. Glenn, D. E. Burton, H. L. McKague, and J. T. Rambo, *Calculational Examination of the Baneberry Event*, Lawrence Livermore Laboratory, Livermore, Calif., UCRL-52365 (1977).
5. R. W. Terhune and H. D. Glenn, *Estimate of Earth Media Shear Strength at the Nevada Test Site*, Lawrence Livermore Laboratory, Livermore, Calif., UCRL-52358 (1977).
6. M. S. Costantino, private communication (1979).
7. N. Howard, private communication (1979).
8. R. C. Schroeder, *A Comparison of Initial Conditions for Nuclear Explosion Calculations*, Lawrence Livermore Laboratory, Livermore, Calif., UCRL-51671 (1974).

GDV/ew